

# Hubbard model: Pinning of occupation numbers and role of symmetries

Christian Schilling<sup>1,\*</sup>

<sup>1</sup>Clarendon Laboratory, University of Oxford, Parks Road, Oxford OX1 3PU, United Kingdom

(Dated: September 23, 2018)

Fermionic natural occupation numbers do not only obey Pauli's exclusion principle, but are even further restricted by so-called generalized Pauli constraints. Such restrictions are particularly relevant whenever they are saturated by given natural occupation numbers  $\vec{\lambda} = (\lambda_i)$ . For few-site Hubbard models we explore the occurrence of this pinning effect. By varying the on-site interaction  $U$  for the fermions we find sharp transitions from pinning of  $\vec{\lambda}$  to the boundary of the allowed region to nonpinning. We analyze the origin of this phenomenon which turns out to be either a crossing of natural occupation numbers  $\lambda_i(U), \lambda_{i+1}(U)$  or a crossing of  $N$ -particle energies. Furthermore, we emphasize the relevance of symmetries for the occurrence of pinning. Based on recent progress in the field of ultracold atoms our findings suggest an experimental set-up for the realization of the pinning effect.

PACS numbers: 03.65.-w, 05.30.Fk, 31.15.aq, 67.85.-d

## I. INTRODUCTION

The Hubbard model is one of the most important paradigmatic models in solid state physics. It provides important insights into the Mott-Hubbard metal-insulator transition (see e.g. [1, 2]), quantum phase transitions [3], antiferromagnetism, ferrimagnetism, ferromagnetism (see e.g. [4, 5]), the Tomonaga-Luttinger liquid (see e.g. [6]), superconductivity (see e.g. [7]), etc.. For mathematically rigorous results on various properties of the Hubbard model the reader may consult the review Ref. [8] and specifically for the 1-dimensional case the textbook [9]. Since the development of optical lattices and ultracold fermionic gases used to simulate and investigate condensed matter phenomena [10] it also plays an important role in the field of cold atoms. In this context toolboxes were derived that allow to map optical lattice systems to corresponding Hubbard models and vice versa [11, 12]. Besides the application of the Hubbard model for macroscopic systems in solid state physics it has also been used on a microscopic scale to describe the behavior of electrons in molecules as, e.g., for  $H_2$  [13],  $C_{20}$  [14], carbon nanotubes [15] or for the hopping of ultracold fermionic atoms between just a few harmonic traps [16]. In recent years, such microscopic systems are gaining importance since they provide a playground for the study of the crossover from few-fermion to many-fermion physics (see e.g. [17], [18]). In particular the question whether properties of many-fermion systems are already present for microscopically small particle numbers is of great interest.

The physical phenomena mentioned above and governed by the Hubbard model strongly rely on the fermionic exchange statistics. This condition on the  $N$ -fermion quantum state  $|\Psi\rangle$  derived by Heisenberg and Dirac [19, 20] implies the famous Pauli exclusion principle [21], the restriction of fermionic occupation numbers,

$$0 \leq n_i \leq 1, \forall i. \quad (1)$$

Here,  $n_i$  denotes the particle number expectation values for 1-particle states labeled by  $i$ . From this 1-particle viewpoint the strong influence of Pauli's exclusion principle for fermionic systems is not surprising. Since it prevents a fermion from hopping to a neighboring lattice site which is already occupied by another fermion in the same spin state it can restrict the mobility of fermions significantly.

In a seminal paper, Borland and Dennis [22] for  $N = 3, 4$  identical fermions and a 1-particle Hilbert space with dimensions  $d = 6, 7, 8$  have shown that the fermionic exchange statistics does not only imply Pauli's exclusion principle but leads to even stronger restrictions on fermionic natural occupation numbers. Only recently, Klyachko and Altunbulak [23–25] have found a general framework based on algebraic topology which allows to determine for each given pair  $(N, d)$  all additional restrictions. To be more specific we consider a system of  $N$ -identical fermions with an underlying  $d$ -dimensional 1-particle Hilbert space  $\mathcal{H}_1^{(d)}$ . The  $N$ -fermion quantum states are given by antisymmetric states  $|\Psi\rangle \in \wedge^N [\mathcal{H}_1^{(d)}]$ . To each such state we can assign its *natural occupation numbers* (NON)  $\lambda_i$ , the eigenvalues of the corresponding 1-particle reduced density operator (1-RDO)

$$\hat{\rho}_1 \equiv N \text{Tr}_{N-1} [|\Psi\rangle \langle \Psi|] = \sum_{k=1}^d \lambda_k |k\rangle \langle k|, \quad (2)$$

obtained by tracing out  $N - 1$  fermions and its eigenstates,  $|k\rangle$ , are called *natural orbitals* (NO). Note, that the implicit dependence of  $\lambda_k$  and  $|k\rangle$  on  $\hat{\rho}_1$  and  $|\Psi\rangle$ , respectively, is suppressed. The Pauli exclusion principle (1) can be reformulated as

$$0 \leq \lambda_i \leq 1, \forall i. \quad (3)$$

For each given pair  $(N, d)$  the *generalized Pauli constraints* (GPC) are given by finitely many affine restrictions [23–25]

$$D_j^{(N,d)}(\vec{\lambda}) \equiv \kappa_j^{(0)} + \sum_{i=1}^d \kappa_j^{(i)} \lambda_i \geq 0, \quad (4)$$

\*Electronic address: christian.schilling@physics.ox.ac.uk

$\kappa_j^{(i)} \in \mathbb{Z}$ ,  $j = 1, \dots, r_{N,d}$  giving rise to a polytope  $\mathcal{P}_{N,d} \subset \mathbb{R}^d$  of allowed vectors  $\vec{\lambda} = (\lambda_i)_{i=1}^d$  of decreasingly-ordered NON. Since this polytope  $\mathcal{P}_{N,d}$  is a proper subset of the ‘Pauli hypercube’  $[0, 1]^d$  described by (3) the GPC are more restrictive than Pauli’s exclusion principle.

Particular importance of these GPC is expected if a given quantum system’s NON are saturating one or more GPC, i.e.  $\vec{\lambda}$  lies on the boundary of  $\mathcal{P}_{N,d}$ . This pinning effect was suggested by Klyachko [26] and physical consequences have been explained in Refs. [26, 27]. Pinning as effect in the 1-particle picture is particularly relevant since it allows to reconstruct the structure of the corresponding  $N$ -fermion quantum state  $|\Psi\rangle$  [26]. Even more, it leads to a significant simplification of  $|\Psi\rangle$  being represented by a linear superposition of a much smaller subset of allowed Slater determinants. However, these rigorous structural implications are also the reason why pinning is not expected to show up in most realistic physical systems [28]. Prior analytic results for fully polarized fermions in a harmonic trap up to medium interaction strengths [29] provide evidence for that expectation. There, although the vector  $\vec{\lambda}$  of NON for the ground state was not lying on a facet of the polytope  $\mathcal{P}_{N,d}$  (i.e. it is not pinned) it was very close to its boundary. The occurrence of this quasipinning effect [29, 30] is also relevant since the structural implication of pinning for the corresponding  $|\Psi\rangle$  still holds approximately [28].

The results in Refs. [26, 29] have motivated further investigations of the role of the GPC in general [31, 32], and of possible quasipinning in particular [33–35]. For instance, the study of atoms and molecules based on only three or maximally four orbitals has shown pinning or quasipinning as well [33–35]. However, to explore quasipinning for atoms and molecules conclusively their ground states have to be known very precisely. This requires significantly more orbitals to capture all the correlations. Based on this and the fact that approximated results hardly allow to distinguish pinning from strong quasipinning, analytic or exact numerical approaches are strongly desirable. The Hubbard model which we are going to study allows for such exact solutions and on the other hand it can be realized by experimental setups for few,  $N$ , fermions on a 1-dimensional lattice with  $r$  sites. The corresponding Hamiltonian (in second quantization) reads

$$\hat{H} = -t \sum_{i=0}^{r-1} \sum_{\sigma} \left( c_{i+1,\sigma}^\dagger c_{i,\sigma} + \text{h.c.} \right) + U \sum_{i=0}^{r-1} \hat{n}_{i\uparrow} \hat{n}_{i\downarrow} \quad (5)$$

where  $c_{i\sigma}^\dagger$  and  $c_{i\sigma}$  are the fermionic creation and annihilation operators for a spin- $\frac{1}{2}$  fermion on the  $i$ -th lattice site with spin  $\sigma = \uparrow, \downarrow$  w.r.t. the  $z$ -axis. Moreover,  $\hat{n}_{i\sigma} \equiv c_{i\sigma}^\dagger c_{i\sigma}$  is the particle number operator for a fermion on site  $i$  with spin  $\sigma$ . The first term of this Hamiltonian describes the nearest neighbor hopping of the fermions with hopping constant  $t$  and the second one, the so-called Hubbard term with coupling constant  $U$ , accounts for the Coulombic interaction, restricted to fermions at the same site. In the following, we use the dimensionless Hubbard parameter  $u = U/t$ , set  $t = 1$  and choose periodic boundary conditions. The Hubbard model possesses

various symmetries (see e.g. Ref. [36]). For Hamiltonian (5) we will demonstrate that these symmetries are strongly related with the occurrence of *pinning*.

The paper is organized as follows. In Sec. II we list the various symmetries of the Hamiltonian (5) and introduce a symmetry-adapted basis of  $N$ -fermion quantum states. The main results are presented in Sec. III where we analytically determine the eigenstates of the Hubbard model for three fermions on three lattice sites and explore possible (quasi)pinning. This is extended by an exact numerical approach for the next larger settings involving more fermions and/or more lattice sites in Sec. IV. In Sec. V we emphasize the physical relevance of our findings and comment on possible experimental realizations.

## II. SYMMETRIES

In this section we present the most elementary symmetries of the Hubbard model (5) and introduce a basis of symmetry-adapted quantum states.

Since the symmetries of the Hubbard model are well-known (see e.g. Ref. [36]), they are just listed in order to keep our paper self-contained. First of all, since the Hamiltonian  $\hat{H}$  commutes with the total fermion number operator  $\hat{N} = \sum_{i=0}^{r-1} \sum_{\sigma} \hat{n}_{i,\sigma}$ ,  $[\hat{H}, \hat{N}] = 0$ , the total particle number  $N$  is conserved and we restrict to fixed fermion numbers  $N$ . By employing first quantization in the following  $\hat{H}$  is then restricted to the corresponding  $N$ -fermion Hilbert space  $\mathcal{H}_N \equiv \wedge^N [\mathcal{H}_1]$  of antisymmetric quantum states, where the  $2r$ -dimensional 1-particle Hilbert space has the substructure  $\mathcal{H}_1 = \mathcal{H}_1^{(l)} \otimes \mathcal{H}_1^{(s)}$ . Here,  $\mathcal{H}_1^{(l)} \cong \mathbb{C}^r$  describes the spatial ( $l$ ) degrees of freedom and  $\mathcal{H}_1^{(s)} \cong \mathbb{C}^2$  is the spin Hilbert space of a single fermion.

We denote the total spin vector operator by  $\hat{\vec{S}}$ , its  $z$ -component by  $\hat{S}_z$  and let  $\hat{T}$  be the translation operator which translates each of the  $N$  fermions from its lattice sites  $i$  to the next site  $i + 1$ . Then, the symmetries of  $\hat{H}$  are described by the following relations (see e.g. [36])

$$[\hat{H}, \hat{\vec{S}}^2] = 0, \quad [\hat{H}, \hat{S}_z] = 0, \quad [\hat{H}, \hat{T}] = 0. \quad (6)$$

The operators  $\hat{\vec{S}}^2$ ,  $\hat{S}_z$  and  $\hat{T}$  also commute with each other. Consequently, the total spin quantum number  $S$ , the magnetic spin quantum number  $M$  and the total Bloch number (wave number)  $K$  are good quantum numbers [41]. The Hamiltonian (5) is block diagonal w.r.t. those symmetries and the total Hilbert space splits according to

$$\mathcal{H}_N \equiv \wedge^N [\mathcal{H}_1^{(l)} \otimes \mathcal{H}_1^{(s)}] = \bigoplus_{S=S_-}^{S_+} \bigoplus_{M=-S}^S \bigoplus_{K=0}^{r-1} \mathcal{H}_{S,M,K}. \quad (7)$$

By setting  $\hbar \equiv 1$  the maximal total spin is given by  $S_+ = \frac{N}{2}$  and the minimal total spin  $S_-$  by 0 for  $N$  even and  $\frac{1}{2}$  for  $N$  odd.

Since we will focus below on the 1-fermion picture it is worth noticing that 1-RDO inherit symmetries from the corresponding  $N$ -fermion quantum states  $|\Psi\rangle$  [37]. Whenever  $|\Psi\rangle$  has a symmetry,  $\hat{F}_1^{\otimes N}|\Psi\rangle = e^{i\varphi}|\Psi\rangle$ , where  $\hat{F}_1$  is a 1-fermion operator acting on  $\mathcal{H}_1$ , the corresponding 1-RDO  $\hat{\rho}_1$  inherits the same symmetry,  $[\hat{\rho}_1, \hat{F}_1] = 0$  and is therefore block-diagonal w.r.t. the  $\hat{F}_1$ -eigenspaces.

For the Hubbard model with periodic boundary conditions, the lattice translation  $\hat{T} = \hat{T}_1^{\otimes N}$  defines such a symmetry, where  $\hat{T}_1$  is the 1-fermion translation operator. Another symmetry is generated by the  $z$ -component of the fermion spin. Consequently, the NO arising from any symmetry-adapted state  $|\Psi\rangle$ ,  $|\Psi\rangle \in \mathcal{H}_{S,M,K}$ , are given by  $|k\sigma\rangle \equiv |k\rangle \otimes |\sigma\rangle$ . Here  $|k\rangle \in \mathcal{H}_1^{(l)}$ ,  $k = 0, 1, \dots, r-1$  is the corresponding Bloch state,  $\hat{T}_1|k\rangle = e^{\frac{2\pi}{r}ik}|k\rangle$ , and  $|\sigma\rangle \in \mathcal{H}_1^{(s)}$ ,  $\sigma = \uparrow, \downarrow$ , is the corresponding spin state. Moreover, since  $\hat{\rho}_1$  is diagonal w.r.t. the NO, we can easily calculate the NON. They are given by the diagonal elements  $\langle k\sigma|\hat{\rho}_1|k\sigma\rangle$ .

The basis  $\{|k\sigma\rangle\}$  for  $\mathcal{H}_1$  induces a basis for the  $N$ -fermion Hilbert space  $\mathcal{H}_N$ , the  $N$ -fermion Slater determinants

$$|k_1\sigma_1, \dots, k_N\sigma_N\rangle \equiv \mathcal{A}_N [|k_1\sigma_1\rangle \otimes \dots \otimes |k_N\sigma_N\rangle], \quad (8)$$

where  $\mathcal{A}_N$  is the  $N$ -particle antisymmetrizing operator and the ordering of the 1-particle basis states is given by  $|0\uparrow\rangle, |0\downarrow\rangle, |1\uparrow\rangle, \dots, |r-1\downarrow\rangle$ .

### III. THREE FERMIONS ON THREE SITES

In this section we study the Hubbard model (5) for three fermions on three lattice sites with periodic boundary conditions [42]. We analytically diagonalize the Hamiltonian and explore whether its eigenstates exhibit the pinning or quasipinning effect.

#### A. Analytic diagonalization of the Hamiltonian

To diagonalize (5) on the corresponding  $\binom{6}{3} = 20$ -dimensional 3-fermion Hilbert space we first block-diagonalize  $\hat{H}$  w.r.t. to its symmetries which were mentioned in Sec. II. The total spin quantum number  $S$  can take the two values  $S = \frac{3}{2}, \frac{1}{2}$ . We first split the total Hilbert space w.r.t. those two values for  $S$  and then continue with the magnetic quantum number  $M$ :

- $S = \frac{3}{2}$ . The only state with maximal magnetic quantum number  $M = \frac{3}{2}$  is the symmetry-adapted state  $|0\uparrow, 1\uparrow, 2\uparrow\rangle$ . It has the Bloch number  $K = 0 + 1 + 2 \pmod{3} = 0$ . By successively applying the lowering ladder operator to that state we find the remaining three symmetry-adapted states of the corresponding quadruplet. They read  $\frac{1}{\sqrt{3}}[|0\downarrow, 1\uparrow, 2\uparrow\rangle + |0\uparrow, 1\downarrow, 2\uparrow\rangle + |0\uparrow, 1\uparrow, 2\downarrow\rangle]$ ,  $\frac{1}{\sqrt{3}}[|0\downarrow, 1\downarrow, 2\uparrow\rangle + |0\downarrow, 1\uparrow, 2\downarrow\rangle + |0\uparrow, 1\downarrow, 2\downarrow\rangle]$  and  $|0\downarrow, 1\downarrow, 2\downarrow\rangle$ . As an elementary exercise one verifies that

(5) restricted to that 4-dimensional subspace is given by  $\hat{H}|_{S=\frac{3}{2}} = 0$ .

- $S = \frac{1}{2}$ . The corresponding subspace is 16-dimensional. Since the Hamiltonian is also invariant under simultaneous flips of all spins w.r.t. the  $z$ -axis, we restrict without loss of generality to  $M > 0$ , i.e.  $M = \frac{1}{2}$ .

- $M = \frac{1}{2}$ . In this 8-dimensional subspace we find two states with  $K = 0$ ,  $\frac{1}{\sqrt{3}}[|0\downarrow, 1\uparrow, 2\uparrow\rangle + e^{\pm\frac{2\pi}{3}i}|0\uparrow, 1\downarrow, 2\uparrow\rangle + e^{\mp\frac{2\pi}{3}i}|0\uparrow, 1\uparrow, 2\downarrow\rangle]$ , and the Hamiltonian restricted to that 2-dimensional subspace,  $\mathcal{H}_{\frac{1}{2}, \frac{1}{2}, 0}$ , is given by  $u \mathbf{1}_2$ . The remaining subspaces are  $\mathcal{H}_{\frac{1}{2}, \frac{1}{2}, 1}$  and  $\mathcal{H}_{\frac{1}{2}, \frac{1}{2}, 2}$ . However, due to the additional invariance of  $\hat{H}$  under inversion in the reciprocal lattice (recall that  $K = 2$  equals  $K = -1$ ), we can restrict to the case  $K = 1$ . This subspace is spanned by the three states  $|0\uparrow, 0\downarrow, 1\uparrow\rangle, |1\uparrow, 1\downarrow, 2\uparrow\rangle$  and  $|0\uparrow, 2\uparrow, 2\downarrow\rangle$  and  $\hat{H}$  represented w.r.t. to those three states takes the form

$$\hat{H}|_{\mathcal{H}_{\frac{1}{2}, \frac{1}{2}, 1}} = \begin{pmatrix} \frac{2u}{3} - 3 & -\frac{u}{3} & -\frac{u}{3} \\ -\frac{u}{3} & \frac{2u}{3} + 3 & -\frac{u}{3} \\ -\frac{u}{3} & -\frac{u}{3} & \frac{2u}{3} \end{pmatrix}. \quad (9)$$

The diagonalization of this  $3 \times 3$ -matrix leads to a cubic equation which is presented and solved in Appendix A.

- $M = -\frac{1}{2}$ . Results are identical to the case  $M = \frac{1}{2}$  up to a simultaneous flip of all three spins w.r.t. the  $z$ -axis.

This completes the diagonalization of the Hubbard Hamiltonian (5).

The energy spectrum of  $\hat{H}$  is shown in Fig. 1. The three

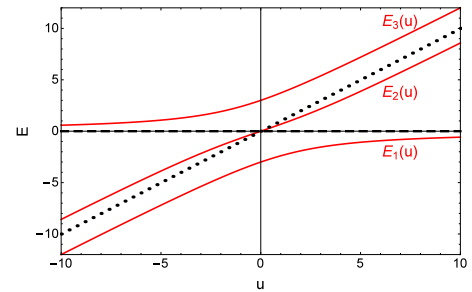


FIG. 1: Energy spectrum for the 3-site Hubbard model for three spin- $\frac{1}{2}$  fermions. Each eigenvalue has multiplicity four. The dashed black line (horizontal line) corresponds to  $S = \frac{3}{2}$ . The case  $S = \frac{1}{2}$  yields the black straight dotted line ( $K = 0$ ) and the three red solid lines correspond to the solution for the nontrivial subspace problem (9) for  $K = \pm 1$ .

solid lines  $E_1(u), E_2(u)$  and  $E_3(u)$  are those arising from the eigenvalue problem for (9),

$$\hat{H}|_{\mathcal{H}_{\frac{1}{2}, \frac{1}{2}, 1}} |\Psi_j(u)\rangle = E_j(u) |\Psi_j(u)\rangle, \quad j = 1, 2, 3. \quad (10)$$

According to the symmetries each  $E_j(u)$  has multiplicity four (quantum numbers  $S = \frac{1}{2}$ ,  $M = \pm\frac{1}{2}$  and  $K = \pm 1$ ). For the four eigenstates with  $S = \frac{3}{2}$  we find the eigenvalue  $E(u) \equiv 0$  (dashed line) and for those with  $S = \frac{1}{2}$ ,  $M = \pm\frac{1}{2}$  and  $K = 0$ ,  $E(u) = u$  (dotted line).

### B. Pinning analysis

In this section we investigate whether the energy eigenstates of the Hubbard Hamiltonian are showing quasipinning or pinning. Due to their particular relevance for experiments we first consider symmetry-adapted states. At the end of this section we also study coherent superposition of degenerate eigenstates.

The corresponding GPC (cf. Eq. (4)) for the setting of  $N = 3$  fermions and a 6-dimensional 1-particle Hilbert space are given by [22]

$$\begin{aligned} \lambda_1 + \lambda_6 &= \lambda_2 + \lambda_5 = \lambda_3 + \lambda_4 = 1 \\ D^{(3,6)}(\vec{\lambda}) &\equiv \lambda_5 + \lambda_6 - \lambda_4 \geq 0. \end{aligned} \quad (11)$$

The first three GPC lead to strong structural implications for the corresponding 3-fermion quantum state (see e.g. [28]). Since they are always saturated it only makes sense to explore a possible saturation of the fourth constraint, which takes the form of a proper inequality.

First, we study the four eigenstates with  $S = \frac{3}{2}$ . Those two with a minimal/maximal  $M$  are *single* Slater determinants and consequently their NON equal the Hartree-Fock point  $\vec{\lambda}_{HF} = (1, 1, 1, 0, 0, 0)$ . Since this vector even saturates the weaker Pauli exclusion principle constraint (1) it is also trivially pinned to the polytope boundary. The other two eigenstates, those with  $M = \pm\frac{1}{2}$ , have NON  $\frac{1}{3}(2, 2, 2, 1, 1, 1)$  which is not pinned. This example also demonstrates that NON of degenerate energy eigenstates can be quite different.

Now, we continue with the  $S = \frac{1}{2}$ -eigenstates. Those four with  $K = 0$  also do not depend on  $u$  and their NON are given again by  $\frac{1}{3}(2, 2, 2, 1, 1, 1)$ . More interesting are the remaining three eigenstates (with multiplicity four) arising from (9) and (10), since they do depend on  $u$ . These states have the general form

$$\begin{aligned} |\Psi(u)\rangle &= \alpha(u)|0\uparrow, 0\downarrow, 1\uparrow\rangle + \beta(u)|1\uparrow, 1\downarrow, 2\uparrow\rangle \\ &+ \gamma(u)|0\uparrow, 2\uparrow, 2\downarrow\rangle. \end{aligned} \quad (12)$$

The three coefficients  $\alpha(u)$ ,  $\beta(u)$  and  $\gamma(u)$  are calculated in Appendix A and their absolute squares are presented in Fig. 2 for the three non-trivial eigenstates following from (10).

The corresponding 1-particle density operator represented w.r.t. to the 1-particle states  $|k\sigma\rangle$  is diagonal as explained in Sec. II. In particular, this means that the two different spin-blocks are decoupled [43], i.e.

$$\hat{\rho}_1 = \hat{\rho}_1^\uparrow \oplus \hat{\rho}_1^\downarrow. \quad (13)$$

Since  $\hat{\rho}_1$  is normalized to  $N = 3$  and needs to reproduce the  $S_z$ -spin expectation value  $M = \frac{1}{2}$  the blocks have the specific normalizations  $\text{Tr}[\hat{\rho}_1^\uparrow] = 2$  and  $\text{Tr}[\hat{\rho}_1^\downarrow] = 1$ .

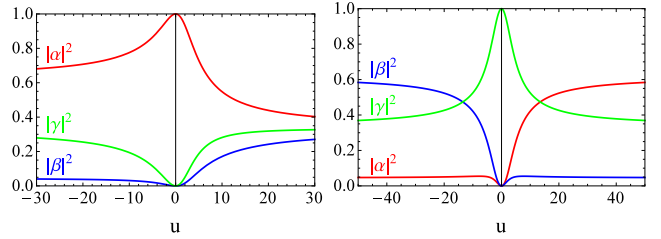


FIG. 2: The absolute squares of the coefficients  $\alpha(u)$  (red),  $\beta(u)$  (blue) and  $\gamma(u)$  (green) for the eigenstates following from (10). Those for the ground state  $|\Psi_1(u)\rangle$  (left) are identical to those for the highest energy state  $|\Psi_3(u)\rangle$  (not shown) up to a reflection w.r.t. the vertical axis. On the right the corresponding result for the excited state  $|\Psi_2(u)\rangle$  is shown.

For the eigenvalues  $n_k^{\uparrow/\downarrow}$ ,  $k = 0, 1, 2$  of  $\hat{\rho}_1^{\uparrow/\downarrow}$  corresponding to the natural orbitals  $|k, \uparrow / \downarrow\rangle$  we find

$$\begin{aligned} n_0^\uparrow &= |\alpha(u)|^2 + |\gamma(u)|^2, & n_0^\downarrow &= |\alpha(u)|^2 \\ n_1^\uparrow &= |\alpha(u)|^2 + |\beta(u)|^2, & n_1^\downarrow &= |\beta(u)|^2 \\ n_2^\uparrow &= |\beta(u)|^2 + |\gamma(u)|^2, & n_2^\downarrow &= |\gamma(u)|^2. \end{aligned} \quad (14)$$

The structure of this spectrum – three eigenvalues are given by the weights  $|\alpha|^2$ ,  $|\beta|^2$  and  $|\gamma|^2$  and the other three by sums of two of them – is a consequence of the symmetries, only. The concrete form (beyond the symmetries) of the Hubbard Hamiltonian affects only the weights  $|\alpha(u)|^2$ ,  $|\beta(u)|^2$  and  $|\gamma(u)|^2$ .

Furthermore, it is an elementary exercise [30] to show that the normalization of  $\hat{\rho}_1^\uparrow$  and  $\hat{\rho}_1^\downarrow$  together with the first three GPC (11) implies that the largest two NON,  $\lambda_1$  and  $\lambda_2$ , belong to the block  $\hat{\rho}_1^\uparrow$ , the smallest two NON,  $\lambda_5$  and  $\lambda_6$ , belong to the block  $\hat{\rho}_1^\downarrow$  and the smallest eigenvalue  $n_{min}^\uparrow$  of  $\hat{\rho}_1^\uparrow$  and the largest eigenvalue  $n_{max}^\downarrow$  of  $\hat{\rho}_1^\downarrow$  fulfill

$$n_{min}^\uparrow + n_{max}^\downarrow = 1. \quad (15)$$

Eq. (15) simplifies the pinning analysis and we can distinguish two cases

- $n_{max}^\downarrow \geq n_{min}^\uparrow$ : The fourth-largest NON  $\lambda_4$  is therefore given by  $n_{min}^\uparrow$  and for the second line of Eq. (11) we find

$$\begin{aligned} D^{(3,6)}(\vec{\lambda}) &= \lambda_5 + \lambda_6 - \lambda_4 \\ &= (1 - n_{max}^\downarrow) - n_{min}^\uparrow = 0, \end{aligned} \quad (16)$$

where we used that  $\lambda_5$  and  $\lambda_6$  both belong to  $\hat{\rho}_1^\downarrow$ ,  $\text{Tr}[\hat{\rho}_1^\downarrow] = \lambda_5 + \lambda_6 + n_{max}^\downarrow = 1$  and Eq. (15).

- $n_{max}^\downarrow < n_{min}^\uparrow$ . In a similar way we find for this case

$$\begin{aligned} D^{(3,6)}(\vec{\lambda}) &= (1 - n_{max}^\downarrow) - n_{min}^\uparrow \\ &= n_{min}^\uparrow - n_{max}^\downarrow > 0. \end{aligned} \quad (17)$$

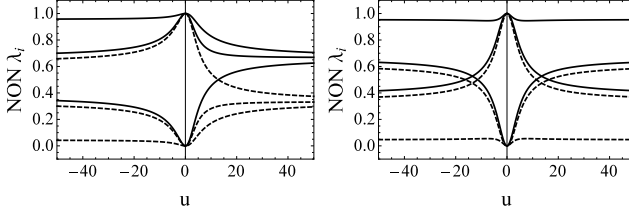


FIG. 3:  $u$ -dependence of the NON  $\lambda_i(u)$  for the ground state  $|\Psi_1(u)\rangle$  (left panel) and for the excited eigenstate  $|\Psi_2(u)\rangle$  (right panel). The NON for the ground state are identical to those for the highest energy state  $|\Psi_3(u)\rangle$  (not shown) up to a reflection w.r.t. the vertical axis. The dashed lines are the NON corresponding to spin  $\downarrow$  and the solid lines correspond to  $\uparrow$ .

This means, depending on the ratio of  $n_{max}^\downarrow$  and  $n_{min}^\uparrow$ , we either have pinning or nonpinning. Whether the eigenstates (12) are pinned or not is illustrated in Fig. 3. It shows the six NON for the relevant on-site interaction regime. The three eigenvalues of the block  $\hat{\rho}_1^\uparrow$  are shown as solid lines and those for  $\hat{\rho}_1^\downarrow$  as dashed lines. Pinning is given for those  $u$ -regimes where  $n_{max}^\downarrow \geq n_{min}^\uparrow$ , i.e. whenever the highest dashed line is above the lowest solid line. E.g. for the ground state  $|\Psi_1(u)\rangle$  presented on the left side of Fig. 3 this is the case for  $u \leq u_0 \approx 12.86$ . At that ‘critical’ point,  $u_0$ , there is a transition from pinning to nonpinning according to the crossing of  $n_{max}^\downarrow(u)$  and  $n_{min}^\uparrow(u)$  [44]. For the excited state  $|\Psi_2(u)\rangle$  presented on the right side we can expect an even more complex behavior, since the relevant NON curves do cross several times.

Indeed, as shown on the upper side of Fig. 4,  $D^{(3,6)}(u)$  for the ground state undergoes a pinning-nonpinning transition.  $D^{(3,6)}(u)$  for the excited state  $|\Psi_2(u)\rangle$  (lower panel of Fig. 4) shows indeed that an expected *reentrance* phenomenon is present, a sequence of pinning-nonpinning transitions.

Due to the distinguished role of the ground state we determine its leading behavior on the right side of the ‘critical’ point  $u_0$ . From the concrete form of the ground state  $|\Psi_1(u)\rangle$  (see Appendix A) one obtains

$$D^{(3,6)}(u) \simeq 0.026(u - u_0), \quad \text{for } u \geq u_0. \quad (18)$$

So far we have restricted ourselves to symmetry-adapted eigenstates. However, since experimental realizations of the Hubbard model typically prepare states with fixed spin quantum numbers (see e.g. [16]) the most general ground state takes the form

$$|\Psi_{\xi,\zeta}(u)\rangle \equiv \xi|\Psi_1(u)\rangle + \zeta\mathcal{I}_Q|\Psi_1(u)\rangle, \quad (19)$$

but has still well-defined spin quantum numbers  $S = \frac{1}{2}$ ,  $M = \pm\frac{1}{2}$ . Here  $|\xi|^2 + |\zeta|^2 = 1$ ,  $\mathcal{I}_Q$  is the 3-fermion inversion operator for the reciprocal ( $Q$ ) lattice and  $|\Psi_1(u)\rangle$  has the form (12) where the coefficients follow from the eigenvalue problem (9) and (10). We set  $\zeta \equiv |\zeta|e^{i\varphi}$  and without loss of generality we choose  $\xi = |\xi| = \sqrt{1 - |\zeta|^2}$ . Due to a  $\frac{2\pi}{3}$ -symmetry of the NON (see Appendix B) we present the pinning results in Fig. 5 for the two extremal cases  $\varphi = 0, \frac{\pi}{3}$ . There we can see that pinning is uniform in  $u$  whenever

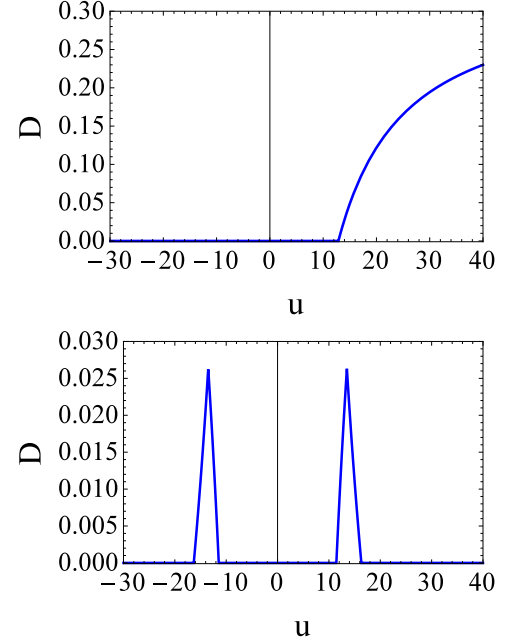


FIG. 4: The eigenstates (10) of the Hubbard model for three fermions on three sites show a pinning-nonpinning transition. The distance  $D^{(3,6)}(u)$  of the NON  $\vec{\lambda}(u)$  to the polytope boundary for the ground state  $|\Psi_1(u)\rangle$  (top) is identical to that for the highest excited state  $|\Psi_3(u)\rangle$  (not shown) up to a reflection  $u \rightarrow -u$ . The excited state  $|\Psi_2(u)\rangle$  (bottom) shows a reentrance behavior of pinning in form of four pinning-nonpinning transition.

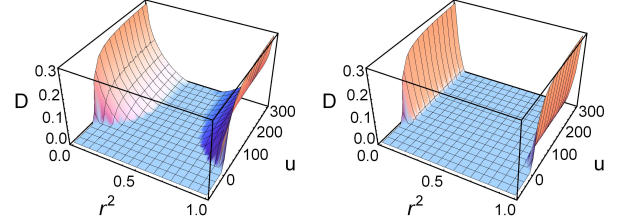


FIG. 5: Saturation  $D(u)$  for the ground state  $|\Psi(u)\rangle = \sqrt{1 - r^2}|\Psi_1(u)\rangle + r e^{i\varphi}\mathcal{I}_Q|\Psi_1(u)\rangle$  of the Hubbard model with three sites and three fermions for the two extremal cases  $\varphi = 0$  (left) and  $\varphi = \frac{\pi}{3}$  (right).

$|\zeta|^2 = |\xi|^2 = r^2 = \frac{1}{2}$ . For all other superpositions it vanishes for some critical value  $u_0(\zeta)$ . Moreover, since this critical value  $u_0(\zeta)$  is minimal for either  $\zeta = 0$  or  $|\zeta| = 1$ , we conclude that superposing  $|\Psi_1(u)\rangle$  and  $\mathcal{I}_Q|\Psi_1(u)\rangle$  extends the  $u$ -regime of pinning from  $(-\infty, 12.86]$  to some larger interval  $(-\infty, u_0(\zeta)]$ ,  $u_0(\zeta) \geq 12.86$ . Furthermore, as already suggested by Fig. 5 it turns out that the relative phase  $\varphi = \frac{\pi}{3}$  favors pinning best.

#### IV. LARGER SETTINGS

In this section we study the next larger systems. However, since complete families of GPC are not known yet for cases

corresponding to more than  $N = 5$  fermions and more than  $r = 5$  lattice sites we restrict to  $N \leq 5$  and  $r \leq 5$ . The GPC for all those cases can be found in [25]. We diagonalize the corresponding Hamiltonians exactly by numerical methods. In the following we present as representative cases the two cases  $(N, r) = (3, 4), (5, 5)$ . The other cases  $(3, 5), (4, 4), (4, 5)$  are qualitatively similar. Note also, that due to the particle-hole symmetry [36], the NON for the cases  $(N, r)$  with  $N > r$  follow from those for  $N < r$ .

### A. Three fermions on four sites

For the Hubbard model with three spin- $\frac{1}{2}$  fermions on four lattice sites we explore possible pinning for several symmetry

adapted eigenstates. In Fig. 6 we present the results, i.e. the minimal distance  $D_{min}(u)$  of the vector  $\vec{\lambda}(u)$  of NON to the polytope boundary  $\partial\mathcal{P}_{3,4}$ , for the 5-dimensional subspace with quantum numbers  $(S, M, K) = (\frac{1}{2}, \frac{1}{2}, 1)$ . The eigenstates for the other subspaces show similar behavior.  $D_{min}(u)$  for the five eigenstates are ordered from the front to the back according to increasing energy. The first and fifth as well as the second and fourth state behave identically up to a reflection of  $u$  at  $u = 0$  [45].  $D_{min}$  for the eigenstate with minimal energy shows transitions between pinning (shown in black) and quasipinning, which is here defined as  $D_{min} \leq 10^{-3}$ . The second eigenstate in this subspace exhibits pinning for negative  $u$ . For positive  $u$  there is a pinning-quasipinning-pinning transition followed by nonpinning for larger  $u$ . The third eigenstate is pinned in the interval  $[-3.75, 3.75]$  and nonpinned in the remaining regime.

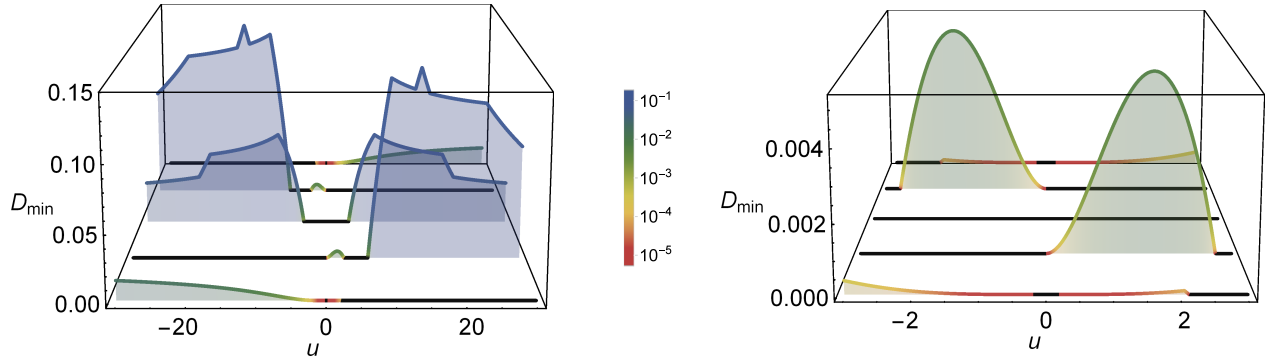


FIG. 6: For the Hubbard model with three fermions on four sites all five eigenstates with quantum numbers  $(S, M, K) = (\frac{1}{2}, \frac{1}{2}, 1)$  are explored w.r.t. possible (quasi)pinning. The curves  $D_{min}(u)$  showing the minimal distance of the NON  $\vec{\lambda}(u)$  to the polytope boundary are ordered according to increasing energy from the front to the back. Pinning is shown in black and the strength of quasipinning is visualized in form of different colors.

It is instructive and also relevant for possible experimental realizations of the pinning effect to study the global ground state separately. For the  $u$ -interval  $(-18.6, 18.6)$  the ground state belongs to the blocks  $(S, M, K) = (\frac{1}{2}, \pm\frac{1}{2}, \pm 1)$  which were already discussed and presented in Fig. 6. At ‘critical’ points  $u \approx \pm 18.6$  energy eigencurves cross and the ground state changes its quantum numbers to  $(S, M, K) = (\frac{1}{2}, \pm\frac{1}{2}, \pm 2)$  for  $u < -18.6$  and  $(S, M, K) = (\frac{3}{2}, \pm\frac{3}{2}, 0), (\frac{3}{2}, \pm\frac{1}{2}, 0)$  for  $u > 18.6$ . The ground state pinning behavior is shown in Fig. 7. The behavior in the regime  $(-18.6, 18.6)$  is already known from Fig. 6 and for  $|u| > 18.6$  there is always pinning. The nonanalytic behavior of the distance  $D_{min}(u)$  of the NON  $\vec{\lambda}(u)$  to the polytope boundary at ‘critical’ points has different origins. First, recall that the Hamiltonian (5) depends analytically on the on-site interaction  $u$  and the energy spectrum and eigenstates inherit this analyticity. However, the ordering of the eigenstates according to increasing energies may violate this analyticity. This happens as already mentioned above at the ‘critical’ point  $u = -18.6$ . At the other ‘critical’ point  $u = +18.6$   $D_{min}(u)$

is analytic since both quantum states whose energy curves are crossing show identical pinning behavior (both are pinned). Even for a given analytic  $N$ -fermion state  $|\Psi(u)\rangle$  nonanalytic behavior of  $D_{min}(u)$  is possible. Although the 1-RDO (recall (2)) and therefore also its spectrum (NON) and NO inherit this analyticity the ordering of the NON  $\lambda_i(u) \geq \lambda_{i+1}(u)$  may violate it and could therefore lead to ‘critical’ points for  $D_{min}(u)$ . This happens at  $u \approx 2.1$  (see inset of Fig. 7). To verify this we study the distances of successive NON and present those three pairs in Fig. 8 which indicate crossings of NON. There is indeed a crossing at  $u \approx 2.1$  since  $\lambda_6 - \lambda_7$  vanishes there. But why do the crossings at  $u = 4.4, 12.1$  indicated in the first two graphics in Fig. 8 not lead to ‘critical’ points for  $D_{min}(u)$ ? The reason is obvious. Crossing of NON has only an influence on  $D_{min}(u)$  if the corresponding two NON do enter  $D_{min}$  differently (recall the form (4)), i.e. with different coefficients  $\kappa_i$ . To verify this for the ground state studied in this section we first need to know the polytope facet which is closest to  $\vec{\lambda}(u)$ , i.e. we need to find the most

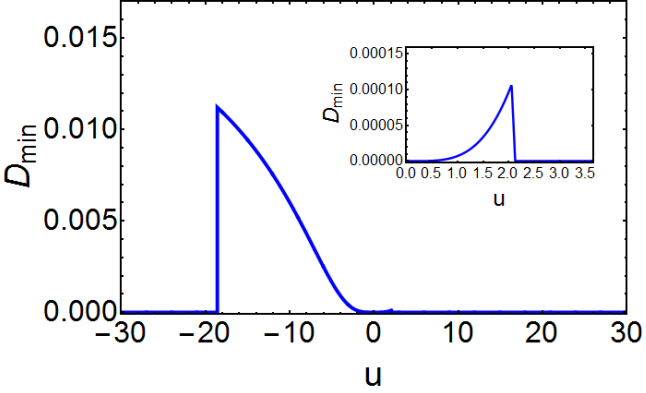


FIG. 7: For the ground state of the Hubbard model with three fermions on four sites possible (quasi)pinning is explored. For very negative on-site interactions  $u$  the ground states exhibits always pinning which vanishes at a ‘critical’ point  $u_1 \approx -18.6$  in form of a sharp pinning-nonpinning transition. Also quasipinning-pinning transitions can be found, namely at the ‘critical’ points  $u_2 = 0$  and  $u_3 \approx 2.1$  (see inset).

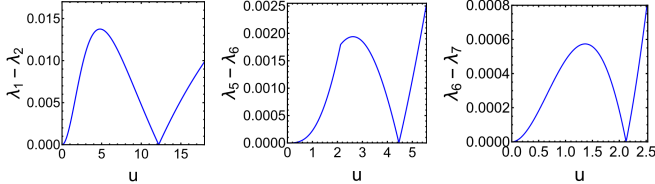


FIG. 8: For the ground state of the Hubbard model with three fermions on four sites only the distances  $\lambda_i(u) - \lambda_{i+1}$  for  $i = 1, 5, 6$  of decreasingly ordered NON  $\lambda_i(u)$  have nonanalytic points. Such nonanalytic behavior for some ‘critical’ values for  $u$  can change the underlying pinning behavior  $D_{min}(u)$  of the ground state as shown in Fig. 7

saturated GPC (4). For  $u \geq 2.0$  this is the constraint

$$D(\vec{\lambda}) = 2 - (\lambda_1 + \lambda_2 + \lambda_4 + \lambda_7) \geq 0. \quad (20)$$

Indeed, the NON  $\lambda_6, \lambda_7$  have different weights,  $\kappa_6 = 0$  and  $\kappa_7 = -1$ . This is not true for the other pairs of NON,  $\lambda_1, \lambda_2$  and  $\lambda_5, \lambda_6$  since  $\kappa_1 = \kappa_2 = -1$  and  $\kappa_5 = \kappa_6 = 0$ . Consequently, the pinning behavior is also analytic around  $u \approx 4.4, 12.1$ . A third reason for nonanalytic behavior of  $D_{min}(u)$  is given when the GPC which is most saturated changes, i.e. we have a crossing of two saturations  $D(u), D'(u)$ . This happens at the point  $u \approx 2.0$  (see sharp kink in the inset of Fig. 7) where the GPC (20) and  $D'(\vec{\lambda}) = 1 - \lambda_1 - \lambda_2 + \lambda_3 \geq 0$  interchange their role as most saturated GPC.

## B. Five fermions on five sites

As a third case we study five fermions on five lattice sites. The ground state (with multiplicity four) belongs to the subspaces  $(S, M, K) = (\frac{1}{2}, \pm\frac{1}{2}, \pm 1)$ . Therefore, we explore possible (quasi)pinning for the eigenstates with  $(S, M, K) =$

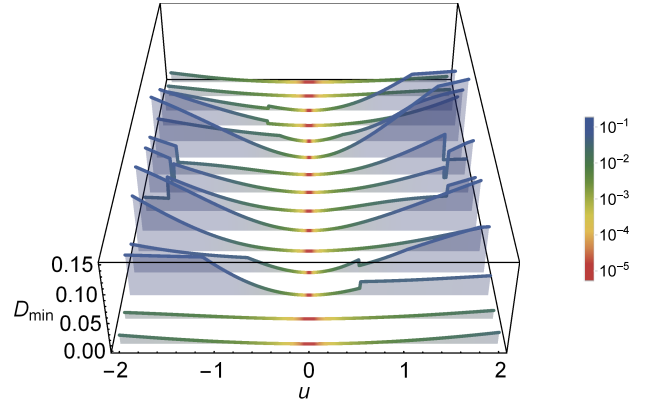


FIG. 9: For the Hubbard model with five fermions on five sites all fifteen eigenstates with quantum numbers  $(S, M, K) = (\frac{1}{2}, \frac{1}{2}, 1)$  are explored w.r.t. possible (quasi)pinning. The curves  $D_{min}(u)$  showing the minimal distance of the NON  $\vec{\lambda}(u)$  to the polytope boundary are ordered according to increasing energy from the front to the back. Pinning is given (for each eigenstate) only for the single point  $u = 0$  (not visible in the graphic) and the strength of quasipinning is visualized in form of different colors. Quasipinning is found for several eigenstates in the neighborhood of  $u = 0$ .

$(\frac{1}{2}, \frac{1}{2}, 1)$ . The results are shown in Fig. 9. The eigenstates are ordered from the front to the back according to increasing energy. In particular, the first curve  $D_{min}(u)$  describes the absolute ground state. For several eigenstates pinning of NON  $\vec{\lambda}$  occurs only for the isolated point  $u = 0$ . In the neighborhood of  $u = 0$  we find quasipinning which eventually changes to nonpinning for  $|u| \gtrsim 0.5$ . The eigenstates of the other subspaces with  $S = \frac{1}{2}$  show very similar behavior as those for  $K = 1$  shown in Fig. 9. For  $S = \frac{3}{2}, \frac{5}{2}$  the corresponding subspaces are much smaller and the pinning behavior shows more transitions similar to the results for  $S = \frac{1}{2}$  for three fermions on four sites presented in Fig. 6.

Finally, it should be also mentioned that linearly superposing degenerate eigenstates belonging to subspaces with different quantum numbers leads again to enhancement of pinning as discussed at the end of Sec. III B.

## V. SUMMARY AND CONCLUSION

The Pauli exclusion principle has a strong impact on the behavior of fermionic quantum systems. It is not commonly known but quite promising that fermionic natural occupation numbers (NON)  $\vec{\lambda} \equiv (\lambda_i)$  are even further restricted by so-called generalized Pauli constraints (GPC) to a polytope  $\mathcal{P}$ , a proper subset of the ‘Pauli hypercube’  $[0, 1]^d$ . Particular physical relevance of those restrictions is given whenever  $\vec{\lambda} \equiv (\lambda_i)$  lies on, or at least very close, to the polytope boundary  $\partial\mathcal{P}$ .

All investigations so far of such possible pinning or quasipinning of NON  $\vec{\lambda}$  to the boundary  $\partial\mathcal{P}$  of the allowed region have considered fermions in a single harmonic trap and atomic systems, only. E.g. a first analytic result has revealed strong

quasipinning [29] for the ground state of a system in a harmonic trap. Here, we studied for the first time, in form of the Hubbard model, a system which is also relevant for condensed matter physics in general and for ultracold fermionic gases in particular. By exactly diagonalizing the Hamiltonian we explored possible pinning for few-site Hubbard models for up to five fermions on five lattice sites and as function of the dimensionless on-site parameter  $u$ .

In contrast to fermions in harmonic traps or in atoms, periodic lattice models with isotropic interaction provide a significant advantage. Due to the translational symmetry the natural orbitals, the eigenvectors of the 1-particle reduced density operator (1-RDO)  $\hat{\rho}_1$ , are known from the very beginning. They are given by the Bloch states  $|k\rangle$  multiplied by a spin state  $|\sigma\rangle$ ,  $\sigma = |\uparrow\rangle, |\downarrow\rangle$ . As a consequence, the NON, the eigenvalues of the 1-RDO, gain physical relevance and can easily be calculated as the diagonal elements  $\langle k\sigma|\hat{\rho}_1|k\sigma\rangle$  of  $\hat{\rho}_1$ .

For all cases  $(N, r)$  with  $N \leq 5$  fermions on  $r \leq 5$  sites we found for many eigenstates finite or even semi-infinite  $u$ -intervals where their NON  $\vec{\lambda}(u)$  are pinned. The end points of those intervals define ‘critical’ points where sharp pinning-nonpinning or pinning-quasipinning transitions are found. As an ‘order parameter’ the minimal distance  $D_{min}(u)$  of  $\vec{\lambda}(u)$  to the polytope boundary  $\partial\mathcal{P}$  has been used. We also studied the origin of those transitions which turns out to be either a crossing of eigenenergies or a crossing of NON  $\lambda_i(u), \lambda_{i+1}(u)$ .

As a further observation we found for the case of degenerate eigenspaces that superposing two symmetry-adapted eigenstates can strongly enhance the  $u$ -regime of pinning.

These findings also shed more light on the occurrence of pinning for other systems. As explained, e.g., in [28], pinning as an effect in the 1-particle picture implies that the corresponding  $N$ -fermion quantum state  $|\Psi\rangle$  has a significantly simplified structure. By expanding  $|\Psi\rangle$  in Slater determinants built up from its own natural orbitals  $|\alpha\rangle$ ,

$$|\Psi\rangle = \sum_{1 \leq \alpha_1 < \dots < \alpha_N \leq d} c_{\alpha_1, \dots, \alpha_N} |\alpha_1, \dots, \alpha_N\rangle, \quad (21)$$

many of the expansion coefficients  $c_{\alpha_1, \dots, \alpha_N}$  need to vanish rigorously, in case of pinning. This is also the reason why pinning is not expected to show up in most realistic quantum systems. However, our work clearly shows that symmetries, as e.g. translational symmetry, cause such a significant reduction of Slater determinants (see e.g. (12)) and eventually can cause pinning. However, our results also show that the presence of symmetries does not automatically imply pinning.

Due to the physical relevance of the Hubbard model also on the microscopic scale our results suggest a first experimental setup to measure the (quasi)pinning effect. By preparing, e.g., three ultracold fermionic atoms in an optical trap with four local minima located at the vertices of a square, the results found in our work could be checked. Indeed, due to recent progress in experimental physics such microscopic setups can be realized and 1-particle occupation numbers can be measured [16][46].

Besides such a direct verification of (quasi)pinning based

on measuring the 1-RDO, more involved experiments exploiting the robustness of pinned NON are possible. To explain this, notice that if a system with NON pinned to the polytope boundary is slightly perturbed the vector  $\vec{\lambda}$  in leading order can move only along the polytope boundary but not perpendicular to it. By changing the on-site interaction for the atoms for a realization of the Hubbard model the pinning-nonpinning transition could be experimentally observed by measuring possible reaction of the fermionic system to external perturbations (as e.g. nonhomogeneous magnetic fields). In case of pinning these reactions can be suppressed.

Since GPC emerge from the antisymmetry, the experimental verification of the pinning effect would also provide additional evidence for the antisymmetry of fermionic wave functions.

*Acknowledgements.*— We would like to thank M. Christandl, P.G.J. van Dongen, D. Gross, D. Jaksch, A. Lopes, M. Rizzi, N. Schuch and J. Whitfield for helpful discussions. We also gratefully acknowledge financial support from the Swiss National Science Foundation (Grant P2EZP2 152190).

## Appendix A: Diagonalization of the subspace Hamiltonian (9)

In this section we solve the eigenvalue problems (10) where the Hamiltonian is given by Eq. (9).

The eigenvalues are the roots of the characteristic polynomial  $P_u(E)$  of (9), i.e. we need to solve the cubic equation

$$P_u(E) = 6u + E(u^2 - 9) - 2E^2u + E^3 = 0. \quad (A1)$$

Since Appendix B requires details on the structure of the roots of cubic equations we present in this section a few more details (see e.g. also [38]) than necessary. For the canonic form

$$x^3 + ax^2 + bx + c = 0 \quad (A2)$$

we first consider the quantities  $Q$  and  $R$ , defined as

$$Q \equiv \frac{a^2 - 3b}{9}, \quad R \equiv \frac{2a^3 - 9ab + 27c}{54}. \quad (A3)$$

By defining

$$\Theta \equiv \arccos\left(R/\sqrt{Q^3}\right) \quad (A4)$$

the three real roots of (A2) follow as

$$x_k = -2\sqrt{Q} \cos\left(\frac{\Theta + 2\pi k}{3}\right) - \frac{a}{3}, \quad k = 0, 1, 2. \quad (A5)$$

For our concrete characteristic polynomial (A1) we have

$$Q = \frac{u^2}{9} + 3, \quad R = \frac{u^3}{27}. \quad (A6)$$

and as real roots (energy eigenvalues)  $E_1(u), E_2(u)$  and  $E_3(u)$  we find

$$E_k = \frac{2}{3} \left\{ u - \sqrt{u^2 + 27} \cos \left[ \frac{1}{3} \arccos \left( u^3 / \sqrt{(u^2 + 27)^3} \right) + \frac{2\pi(1-k)}{3} \right] \right\}.$$

Here, we ordered the eigenvalues differently than in (A5) to be consistent with the labeling in Fig. 1. Notice also the symmetries of these energies,

$$E_1(-u) = -E_3(u) \quad \text{and} \quad E_2(-u) = -E_2(u). \quad (\text{A7})$$

The corresponding unnormalized eigenvectors  $\vec{v}_j(u) \equiv (\tilde{\alpha}_j(u), \tilde{\beta}_j(u), \tilde{\gamma}_j(u))$ ,  $j = 1, 2, 3$  of matrix (9) follow directly from (9). We find

$$\begin{aligned} \tilde{\alpha}_j(u) &= u + 3 - E_j(u) \\ \tilde{\beta}_j(u) &= u - 3 - E_j(u) \\ \tilde{\gamma}_j(u) &= u - 4E_j(u) + \frac{3}{u} [E_j(u)^2 - 9]. \end{aligned} \quad (\text{A8})$$

which after division by  $\sqrt{|\tilde{\alpha}_j(u)|^2 + |\tilde{\beta}_j(u)|^2 + |\tilde{\gamma}_j(u)|^2}$  yields the normalized coefficients of the eigenstates (12).

## Appendix B: Calculation of the NON for the superposition (19)

In this appendix we calculate the NON for the more general ground state (19). Since (19) is not symmetry-adapted to the lattice translation anymore, the corresponding 1-RDO represented w.r.t. the Bloch states  $\{|k, \sigma\rangle\}$  is not diagonal anymore. However, since (19) is still an  $S_z$ -eigenstate, the new NO are still spin eigenstates w.r.t.  $z$ -axis and the 1-RDO splits into blocks according to Eq. (13). The specific normalizations of both blocks together with the three equalities (11) imply again that for each eigenvalue  $n_j^\uparrow$  of  $\hat{\rho}_1^\uparrow$  there exists a corresponding eigenvalue  $n_i^\downarrow$  of  $\hat{\rho}_1^\downarrow$  such that their sum equals one,  $n_j^\uparrow + n_{4-j}^\downarrow = 1$ ,  $j = 1, 2, 3$ , where the triples  $\{n_j^\uparrow\}$  and  $\{n_j^\downarrow\}$  are ordered decreasingly. Hence, it is sufficient for our purpose to diagonalize just the block  $\hat{\rho}_1^\uparrow$ . By representing it w.r.t. the states  $\{|k, \downarrow\rangle\}$  we obtain the following density matrix

$$\hat{\rho}_1^\uparrow = \begin{pmatrix} |\alpha|^2 & -\xi^* \zeta \alpha^* \gamma & -\xi \zeta^* \alpha^* \gamma \\ -\xi \zeta^* \alpha \gamma^* & |\zeta|^2 |\beta|^2 + |\xi|^2 |\gamma|^2 & -\xi^* \zeta |\beta|^2 \\ -\xi^* \zeta \alpha \gamma^* & -\xi \zeta^* |\beta|^2 & |\xi|^2 |\beta|^2 + |\zeta|^2 |\gamma|^2 \end{pmatrix}. \quad (\text{B1})$$

The cubic characteristic polynomial  $p_u(\lambda)$  reads

$$\begin{aligned} p_u(\lambda) &= \lambda^3 + c_2 \lambda^2 + c_1 \lambda + c_0 = 0 \\ c_2 &= -1 \\ c_1 &= |\alpha(u)|^2 |\beta(u)|^2 + |\alpha(u)|^2 |\gamma(u)|^2 + |\beta(u)|^2 |\gamma(u)|^2 \\ &\quad - (2 - 3|\gamma(u)|^2) |\gamma(u)|^2 |\zeta|^2 |\xi|^2 \\ c_0 &= -|\alpha(u)|^2 |\beta(u)|^2 |\gamma(u)|^2 \\ &\quad \times (1 - 3|\zeta|^2 |\xi|^2 - \zeta^3 (\zeta^*)^3 - (\zeta^*)^3 \xi^3). \end{aligned} \quad (\text{B2})$$

Its roots follow immediately from Eqs. (A2), (A3), (A4) and (A5) in Appendix A.

As a consistency check, notice also that according to Eq. (A5) we have in general

$$x_1 + x_2 + x_3 = -c_2 \quad (\text{B3})$$

which takes here the value  $-c_2 = 1 = \text{Tr}[\hat{\rho}_1^\downarrow]$ .

Finally, we comment on  $\xi, \zeta$ -symmetries of  $\hat{\rho}_1^\downarrow$ . First, note that the vector of NON fulfills

$$\vec{\lambda}(u; \zeta, \xi) = \vec{\lambda}(u; \xi, \zeta), \quad (\text{B4})$$

which follows directly from the invariance of (5) w.r.t. inversions in the Brillouin zone and the form (19). Moreover, blocks  $\hat{\rho}_1^\downarrow(u; \xi, \zeta)$  fulfill

$$\hat{\rho}_1^\downarrow(u; \xi, \zeta e^{\frac{2\pi}{3}i}) = U^\dagger \hat{\rho}_1^\downarrow(u; \xi, \zeta) U \quad (\text{B5})$$

with the unitary matrix  $U = \text{diag}(1, e^{-\frac{2\pi}{3}i}, e^{\frac{2\pi}{3}i})$ . The same actually also holds for the second block,  $\hat{\rho}_1^\uparrow$ , which is not stated here. Thus,

$$\vec{\lambda}(u; \xi, \zeta e^{\frac{2\pi}{3}i}) = \vec{\lambda}(u; \xi, \zeta). \quad (\text{B6})$$

---

[1] J. Hubbard, Proc. Roy. Soc. (London) A **281**, 401 (1964).  
[2] A. Georges, G. Kotliar, W. Krauth, and M. Rozenberg, Rev. Mod. Phys. **68**, 13 (1996).  
[3] S. Sachdev, *Quantum Phase Transitions* (Cambridge Univ. Press, Cambridge, 1999).  
[4] A. Auerbach, *Interacting Electrons and Quantum Magnetism* (Springer, New York, 1994).  
[5] P. Fazekas, *Lecture Notes on Electron Correlation and Magnetism*, vol. 5 of *Series in Modern Condensed Matter Physics* (World Scientific Publishing Co., Singapore, 1999).

- [6] A. Tsvelik, *Quantum Field Theory in Condensed Matter Physics* (Cambridge Univ. Press, Cambridge, 1995).
- [7] M. G. Balachandran A.P., Ercolessi E. and S. A.M., *Hubbard Model and Anyon Superconductivity*, vol. 38 of *Lecture Notes in Physics* (World Scientific Publishing Co., Singapore, 1990).
- [8] H. Tasaki, J. Phys. Cond. Matt. **10**, 4353 (1998).
- [9] F. Essler, H. Frahm, F. Göhmann, A. Klümper, and V. Korepin, *The One-Dimensional Hubbard Model* (Cambridge University Press, 2010).
- [10] I. Bloch, J. Dalibard, and W. Zwerger, Rev. Mod. Phys. **80**, 885 (2008).
- [11] D. Jaksch and P. Zoller, Ann. Phys. **315**, 52 (2005).
- [12] R. Walters, G. Cotugno, T. H. Johnson, S. R. Clark, and D. Jaksch, Phys. Rev. A **87**, 043613 (2013).
- [13] B. Alvarez-Fernandez and J. Blanco, Eur. J. Phys. **23**, 11 (2002).
- [14] J. Alfonsi, G. Lanzani, and M. Meneghetti, New J. Phys. **12**, 083009 (2010).
- [15] F. Lin, E. Srensen, C. Kallin, and J. Berlinsky, J. Phys.: Condens. Matter **19**, 456206 (2007).
- [16] S. Murmann, A. Bergschneider, V. Klinkhamer, G. Zürn, T. Lompe, and S. Jochim, Phys. Rev. Lett. **114**, 080402 (2015).
- [17] A. N. Wenz, G. Zurn, M. S., B. I., T. Lompe, and S. Jochim, Science **342**, 457 (2013).
- [18] A. Angelone, M. Campostrini, and E. Vicari, Phys. Rev. A **89**, 023635 (2014).
- [19] W. Heisenberg, Z. Phys. **38**, 411 (1926).
- [20] P. A. M. Dirac, Proc. R. Soc. A **112**, 661 (1926).
- [21] W. Pauli, Z. Phys. **31**, 765 (1925).
- [22] R. Borland and K. Dennis, J. Phys. B **5**, 7 (1972).
- [23] M. Altunbulak and A. Klyachko, Commun. Math. Phys. **282**, 287 (2008).
- [24] A. Klyachko, J. Phys.: Conf. Ser. **36**, 72 (2006).
- [25] M. Altunbulak, Ph.D. thesis, Bilkent University (2008), <http://www.thesis.bilkent.edu.tr/0003572.pdf>.
- [26] A. Klyachko, [quant-ph/0904.2009](https://arxiv.org/abs/0904.2009) (2009).
- [27] C. Schilling, Mathematical Results in Quantum Mechanics **10**, 9789814618144\_0010 (2014).
- [28] C. Schilling, Phys. Rev. A **91**, 022105 (2015).
- [29] C. Schilling, D. Gross, and M. Christandl, Phys. Rev. Lett. **110**, 040404 (2013).
- [30] C. Schilling, Ph.D. thesis, ETH Zurich (2014).
- [31] R. Chakraborty and D. Mazziotti, Phys. Rev. A **91**, 010101 (2015).
- [32] I. Theophilou, N. Lathiotakis, M. Marques, and N. Helbig, The Journal of Chemical Physics **142** (2015).
- [33] C. Benavides-Riveros, J. Gracia-Bondia, and M. Springborg, Phys. Rev. A **88**, 022508 (2013).
- [34] R. Chakraborty and D. Mazziotti, Phys. Rev. A **89**, 042505 (2014).
- [35] C. Benavides-Riveros and M. Springborg, [arXiv:1409.6953](https://arxiv.org/abs/1409.6953) (2014).
- [36] E. Fradkin, *Field theories of condensed matter physics* (Cambridge Univ. Press, Cambridge, 2013).
- [37] E. Davidson, *Reduced Density Matrices in Quantum Chemistry* (Academic Press, New York, 1976).
- [38] M. Abramowitz and I. Stegun, *Handbook of Mathematical Functions with Formulas, Graphs, and Mathematical Tables* (Dover, New York, 1964), ninth dover printing, tenth gpo printing ed.
- [39] K. B. Davis, M. O. Mewes, M. R. Andrews, N. J. van Druten, D. S. Durfee, D. M. Kurn, and W. Ketterle, Phys. Rev. Lett. **75**, 3969 (1995).
- [40] M. H. Anderson, J. R. Ensher, M. R. Matthews, C. E. Wieman, and E. A. Cornell, **269**, 198 (1995).
- [41] The Bloch number  $K$  for the 1-dimensional lattice with  $r$  sites is given in units of  $\frac{2\pi}{a\tau}$  ( $a$  is the lattice constant) and is restricted to the first Brillouin zone, i.e.  $K = 0, 1, \dots, r - 1$  and the corresponding  $\hat{T}$ -eigenstates  $|\Psi_K\rangle$  fulfill  $\hat{T}|\Psi_K\rangle = e^{\frac{2\pi}{\tau}iK}|\Psi_K\rangle$ .
- [42] We do not consider the case of  $N = 2$  fermions since the corresponding GPC take the form of equalities (see e.g. [28]) rather than inequalities and exploring possible pinning is therefore meaningless.
- [43] This holds in general for all  $\hat{S}_z$ -symmetry-adapted  $N$ -fermion quantum states  $|\Psi\rangle \in \wedge^N [\mathcal{H}_1^{(l)} \otimes \mathcal{H}_1^{(s)}]$
- [44] We call points at which  $D(u)$  is nonanalytic in  $u$  ‘critical’ points. Although the physical behavior of the system may change at such points it is not a critical point in the traditional sense as it occurs, e.g., at quantum phase transitions.
- [45] This follows from the  $U(1)$ -gauge transformation  $c_{j\sigma} \rightarrow e^{ij\pi} c_{j\sigma}$  applied to Hamiltonian (5) which transforms  $H(t, U)$  for the case of for an even number of sites into  $-H(t, -U)$ .
- [46] In [16] the occupancies of the lattice sites were measured. It is not clear to us whether their techniques also allow to measure the occupancies in the momentum representation. For bosons such momentum distributions were successfully measured already in 1995 to verify Bose-Einstein condensation [39, 40].